Journal of Applied Electrochemistry **31**: 181–192, 2001.

Use of gaseous Cr species to diagnose surface and bulk process for O_2 reduction in solid oxide fuel cells

S.P. JIANG
CSIRO, Manufacturing Science & Technology, Private Bag 33, Clayton South MDC, Clayton, Victoria 3169, Australia
(correspondence: fax: +61 3 9544 1128, e-mail: san-ping.jiang@cmst.csiro.au)

Received 2 May 2000; accepted in revised form 22 August 2000

Key words: gaseous Cr species, *in situ* diagnostic method, oxygen reduction, reaction kinetics, solid oxide fuel cells

Abstract

Oxygen reduction reactions on Sr-doped $LaMnO_3$ (LSM), Sr-doped $La(Co,Fe)O_3$ (LSCF) and Pt electrodes have been investigated in the absence and presence of gaseous Cr species at 900 °C in air. Gaseous Cr species were introduced by using chromia-forming alloy interconnect in contact with the electrode. In the presence of gaseous Cr species, the electrode processes for the O_2 reduction on LSM and Pt electrode were significantly inhibited while on LSCF electrodes, the inhibiting effect was much smaller. It has been shown that gaseous Cr species primarily inhibited the electrode surface process of the O_2 reduction reaction and the inhibiting effect can be quantitatively related to the oxygen diffusion coefficient of the electrode material. The results demonstrated that gaseous Cr species can be used to distinguish between the surface and bulk process kinetics for the O_2 reduction reaction under solid oxide fuel cells operation conditions.

1. Introduction

Oxygen reduction reaction is one of the most studied reactions in solid oxide fuel cells (SOFC) [1]. This is primarily related to the fact that the selection of cathode materials is critical in achieving high power output and long-term stability of SOFC as the polarization losses due to the O_2 reduction contribute significantly to the overall performance losses especially for SOFC based on thin film electrolytes [2]. Although oxygen surface exchange and oxygen diffusion properties of a material can be accurately measured by techniques such as secondary ion mass spectroscopy and oxygen isotope exchange techniques [3, 4], there is a lack of *in situ* techniques in the determination of adsorbed species on the electrode surface and in particular in the unambiguous separation of the surface and bulk processes for the O_2 reduction under SOFC operation conditions. This may contribute to the considerable debate and discrepancies on the nature of electrode process of the O_2 reduction reaction. For the O_2 reduction on porous Sr-doped $LaMnO_3$ (LSM) electrodes, the rate determining step ranges from diffusion controlled charge transfer process [5], charge transfer on the LSM coated on Gd-doped CeO_2 electrolyte [6], dissociative adsorption of oxygen at low overpotentials and oxygen diffusion through the LSM bulk at high overpotentials [7], surface diffusion of oxygen [8] to bulk diffusion of oxygen [9]. Recently, we investigated the O_2 reduction on LSM electrodes in the presence of chromia-forming alloy interconnect [10, 11]. It was found that at the early stages of the polarization, the O_2 reduction is primarily limited by the surface diffusion of oxygen species on the LSM electrode, similar to that in the absence of chromia-forming alloy, but proceeds at much slower rates due to the inhibiting effect of the gaseous Cr species such as CrO_3. The results indicate that the gaseous Cr species produced from chromia-forming alloy could be used to diagnose the surface and bulk processes of O_2 reduction under SOFC operation conditions. In this paper the application and effectiveness of the gaseous Cr species (e.g., CrO_3) in the identification of the surface and bulk diffusion kinetics for O_2 reduction reaction has been investigated on LSM, Sr-doped $La(Co,Fe)O_3$ (LSCF) and Pt electrodes. LSCF is a well-known mixed ionic and electronic conductor [3] with very high electrochemical activity for the O_2 reduction reactions [12, 13]. On Pt electrodes it has been generally established that the rate limiting steps for the reaction are the surface diffusion of adsorbed oxygen on the Pt surface [14–16].

2. Experimental details

Zirconia electrolyte substrates were prepared from 3 mol% Y_2O_3–ZrO_2 (TZ3Y, Tosoh, Japan) by tape casting, followed by sintering at 1500 °C for 2 h. The

electrolyte thickness was ~150 μm. $La_{0.72}Sr_{0.18}MnO_3$ (LSM) and $La_{0.6}Sr_{0.4}Co_{0.2}Fe_{0.8}O_3$ (LSCF) powders were prepared by co-precipitation, followed by calcination at 1000 °C and 900 °C in air, respectively. XRD analysis confirmed the perovskite structure of the LSM and LSCF powders. LSM electrodes were applied to the TZ3Y electrolyte substrates by screen-printing and fired at 1150 °C in air for 2 h. To avoid the chemical reaction between LSCF and zirconia electrolyte [17], LSCF electrodes were applied to $Ce_{0.8}Sm_{0.2}O_2$ (SDC) electrolyte (~900 μm thick) by screen-printing and fired in place at 950 °C for 2 h prior to the testing. SDC electrolyte substrates were prepared by isopressing SDC powder and sintered at 1400 °C for 2 h. Pt electrode was prepared by slurry painting of Pt paste (Engelhard, 6082) onto TZ3Y electrolyte and fired in place at 900 °C for 2 h before the testing. The coating thickness was about 50 μm for screen-printed LSM and LSCF electrodes and about 1 μm for slurry-painted Pt electrodes. The electrode area was 0.44 cm^2. Pt paste was painted on to other side of the electrolyte disk to make the counter and reference electrodes. The counter electrode was positioned at the center, symmetrical to the working electrode. The reference electrode was painted as a ring around the counter electrode. The gap between the counter electrode and the ring reference electrode was about 4 mm.

Gaseous Cr species were introduced into the electrode system by using chromia-forming alloy (25 w/o Cr, 73 w/o Fe, 0.7 w/o Mn, negligible Si) interconnect coupon (12 mm × 12 mm × 5 mm thick). On one side of the coupon, channels (1.2 mm × 1.2 mm deep) were cut with holes in the center of each channel. Air was directed to the channels through an alumina tube, ensuring the uniform air flow across the whole electrode coating. Two Pt wires were spot-welded to the coupon to serve as voltage and current probes, respectively. There was no Pt mesh placed between the chromia-forming alloy and the electrode coating. In this arrangement, the chromia-forming alloy also acted as a current collector. Air (BOC, industrial grade, moist content $<0.01\%$) was used without further drying. The air flow rate was controlled at 100 ml min^{-1} for both working and counter electrodes. The cell testing configuration is shown in Figure 1. For the experiments without chromia-forming alloy, Pt mesh was used as current collector for the working electrode and a separate sample holder was used to avoid the Cr contamination. Details of the experimental set-up can also be found in [10].

The initial electrochemical behaviour of the LSM, LSCF and Pt electrodes under the cathodic polarization was studied under a constant current of 200 mA cm^{-2} at 900 °C in air. The cathodic polarization potential ($E_{cathode}$) was measured against the Pt air reference electrode, using a data logging device. The current passage was interrupted from time to time to make galvanostatic current interruption (GCI) and electrochemical impedance spectroscopy (EIS) measurements. GCI was carried out using a Keithley high speed voltmeter (194A) and a Keithley current source (228A) [18]. Overpotential (η) and electrode ohmic resistance (R_Ω) between the cathode and the Pt reference electrode were directly measured from the current interruption transition curves. The electrode was equilibrated at open circuit for about 20 min prior to the EIS measurement. EIS was performed on an EG&G electrochemical impedance analyzer (model 6310) at frequency range of 0.1 Hz to 100 kHz with the signal amplitude of 5 mV under open circuit. The electrode interface (polarization) resistance (R_E) was obtained by subtracting the high frequency intercept from the low frequency intercept on the impedance real axis. After the impedance measurement, cathodic current of 200 mA cm^{-2} was applied to the cell again. However, the period associated with the equilibrium at open circuit and the subsequent EIS measurement was omitted in the plot of $E_{cathode}$ against the cathodic current passage time. The microstructure of the electrode in contact with the chromia-forming alloy was

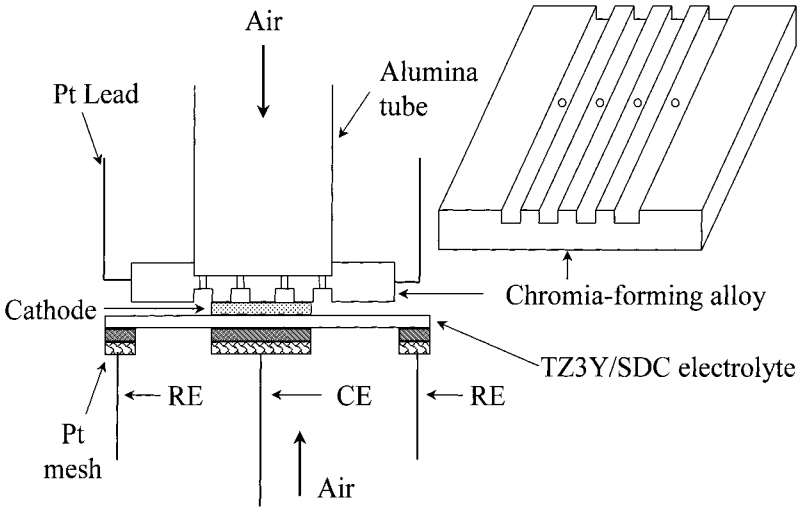

Fig. 1. Test cell arrangement.

examined by scanning electron microscopy (SEM) and X-ray energy dispersive spectroscopy (EDS).

3. Results and discussion

3.1. *SEM micrographs of the electrodes*

Figure 2 shows the SEM micrographs of the LSM, Pt and LSCF electrodes after cathodic polarization at 200 mA cm^{-2} and 900 °C in the presence of chromia-forming alloy. The overall polarization time was 4 h for LSM electrode, 22 h for Pt electrode and 105 h for LSCF electrode. For LSM electrode, there was deposition of fine grains and crystals on the TZ3Y electrolyte surface (Figure 2(a)). EDS analysis indicated that the fine grains were most likely Cr_2O_3 and crystals were $(Cr,Mn)_3O_4$-type spinels [10]. Deposition of Cr species on the LSM electrode surface or inside the electrode body was not detected within the limits of the techniques used. Figure 2(b) is the SEM micrograph of the Pt electrode close to the edge of the electrode. The isolated large particles were Pt particles. EDS analysis indicated that the small and plate-like particles were also Pt particles. Very different from that observed on the LSM electrode, EDS signals associated with chromium were very week, indicating that the deposition of Cr species on the TZ3Y electrolyte surface is negligible. Figure 2(c) shows the SEM micrograph of the LSCF electrode. There were individual particles with distinct crystal facets on the electrolyte and electrode surfaces. EDS analysis identified that the crystals formed on the LSCF electrode surface mainly contained Sr and Cr, probably indicating the formation of $SrCrO_4$ [19, 20]. However, the deposits were random and did not show any preferential deposition either on the electrolyte or on the electrode surface. In all cases, there was no preferential deposition of Cr species on the surface of the electrodes under the conditions studied. The details of the deposition processes of Cr species at LSM, LSCF and Pt electrodes in the presence of chromia-forming alloy interconnect can be found elsewhere [10, 19].

3.2. *Initial electrode behaviour*

Figure 3 shows the initial impedance and polarization responses of a LSM electrode under a cathodic current density of 200 mA cm^{-2} at 900 °C in air in the absence of chromia-forming alloy. Before the current passage, the initial impedance response was characterized by a large and depressed arc and the initial electrode resistance (R_E) was 6.2 Ω cm^2. However, the impedance arcs decreased very quickly with the current passage. For example, after cathodic current passage treatment for 15 min, R_E was reduced to 0.7 Ω cm^2, much smaller than the initial R_E of 6.2 Ω cm^2. The impedance arc was no longer able to recover to the original size before the current passage. The reduction in R_E confirms

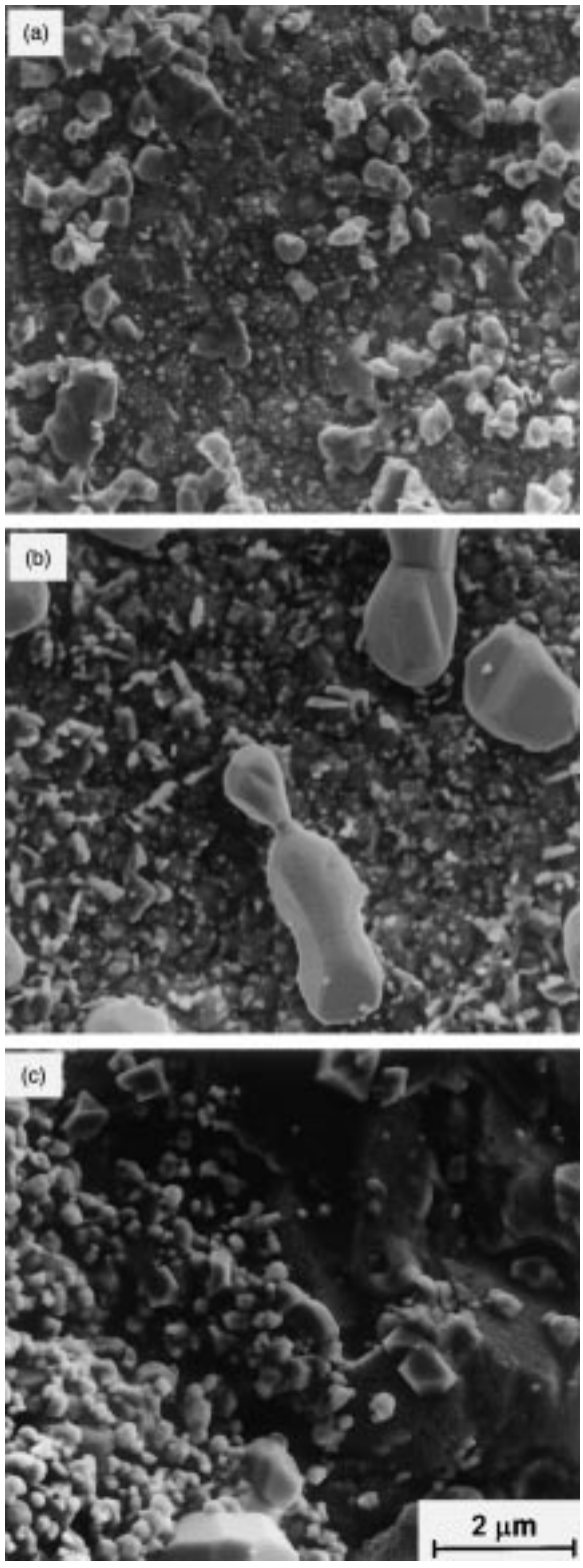

Fig. 2. SEM micrographs of (a) LSM electrode after current passage of 200 mA cm^{-2} and 900 °C for 4 h, (b) Pt electrode after 22 h, and (c) LSCF after 105 h.

the enhancing effect of the cathodic polarization on LSM electrodes for the O_2 reduction reaction [21].

The time behaviour of the cathodic polarization potential ($E_{cathode}$) can be characterized by two distinct potential regions I and II, as shown in Figure 3(b). In

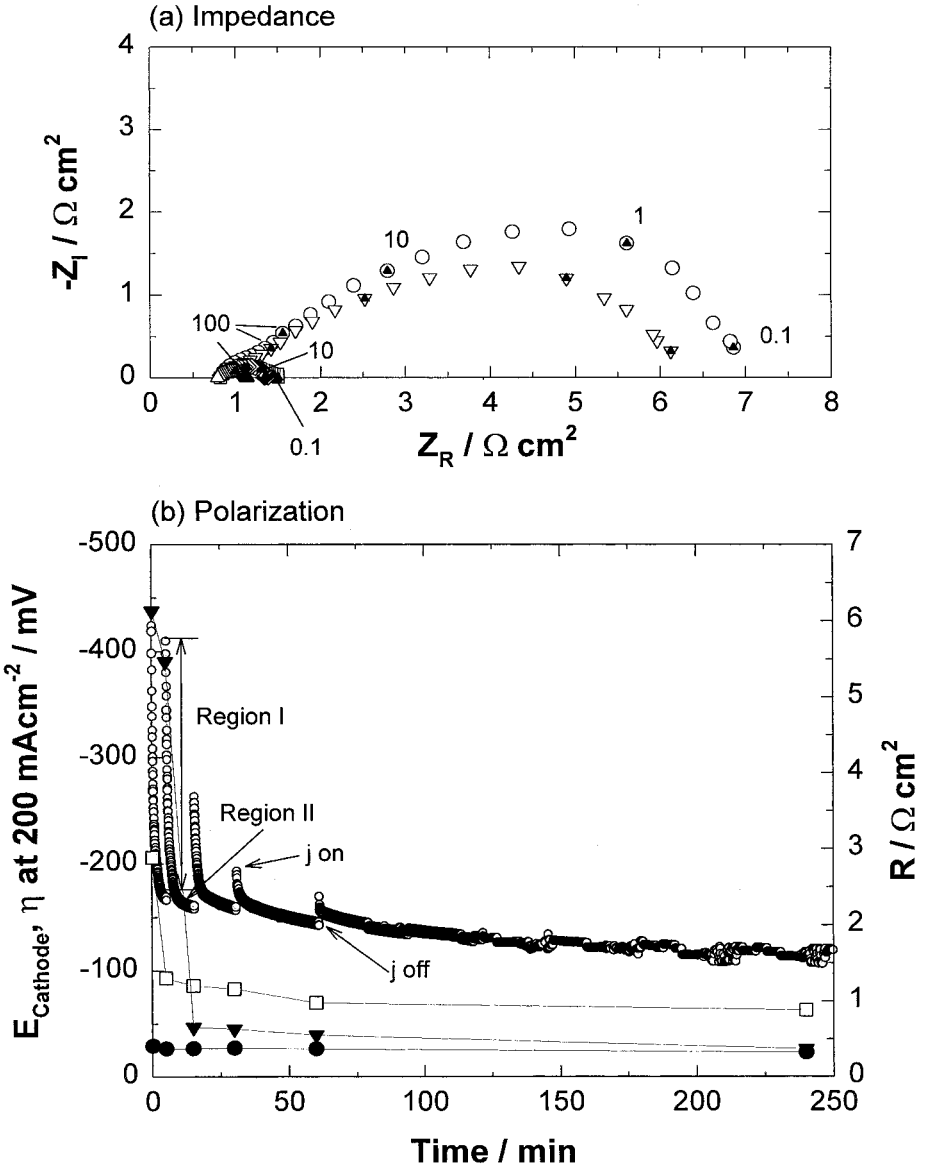

Fig. 3. Initial impedance (a) and polarization (b) curves of a LSM electrode under a cathodic current density of 200 mA cm^{-2} at 900 °C in air in the absence of chromia-forming alloy. Numbers in (a) are frequencies in Hz. Key for (a): (○) 0, (▽) 5, (□) 15, (◇) 60 and (△) 240 min. Key for (b): (○) $E_{cathode}$, (□) η, (●) R_Ω and (▼) R_E.

region I, $E_{cathode}$ decreased very quickly with current passage, reaching region II where the reduction in $E_{cathode}$ was much slower. With applying of a current passage of 200 mA cm^{-2}, $E_{cathode}$ instantly jumped to 424 mV and decreased very rapidly to 166 mV in 5 min. Similar to R_E, the starting value of $E_{cathode}$ decreases very quickly with the current passage. For example, after cathodic current passage for 15 min, the starting $E_{cathode}$ was 264 mV and did not recover to the initial $E_{cathode}$ of 424 mV. Nevertheless, the reduction in region II was much smaller. After current passage for 5 min, $E_{cathode}$ was reduced to 166 mV and after current passage for 60 min, $E_{cathode}$ was reduced to 149 min. GCI data indicated that the reduction in $E_{cathode}$ was due to the reduction in η as R_Ω remained almost the same with the current passage. The polarization behaviour with current passage is in a good agreement with the impedance behaviour for the O_2 reduction in the absence of chromia-forming alloy.

Figure 4 is the initial impedance and polarization responses of a LSM electrode under a cathodic current density of 200 mA cm^{-2} at 900 °C in air in the presence of chromia-forming alloy. In the presence of the chromia-forming alloy, the impedance arcs also decreased with the current passage. However, the reduction in R_E was much smaller compared to that in the absence of chromia-forming alloy. Before the current passage, R_E was 3.9 Ω cm^2 and decreased to 2.7 Ω cm^2 after current passage for 15 min, a reduction of 31%, much smaller than 88% for the R_E reduction in the absence of chromia-forming alloy under the same current passage conditions.

In the presence of chromia-forming alloy, the time behaviour of $E_{cathode}$ can also be characterized by two

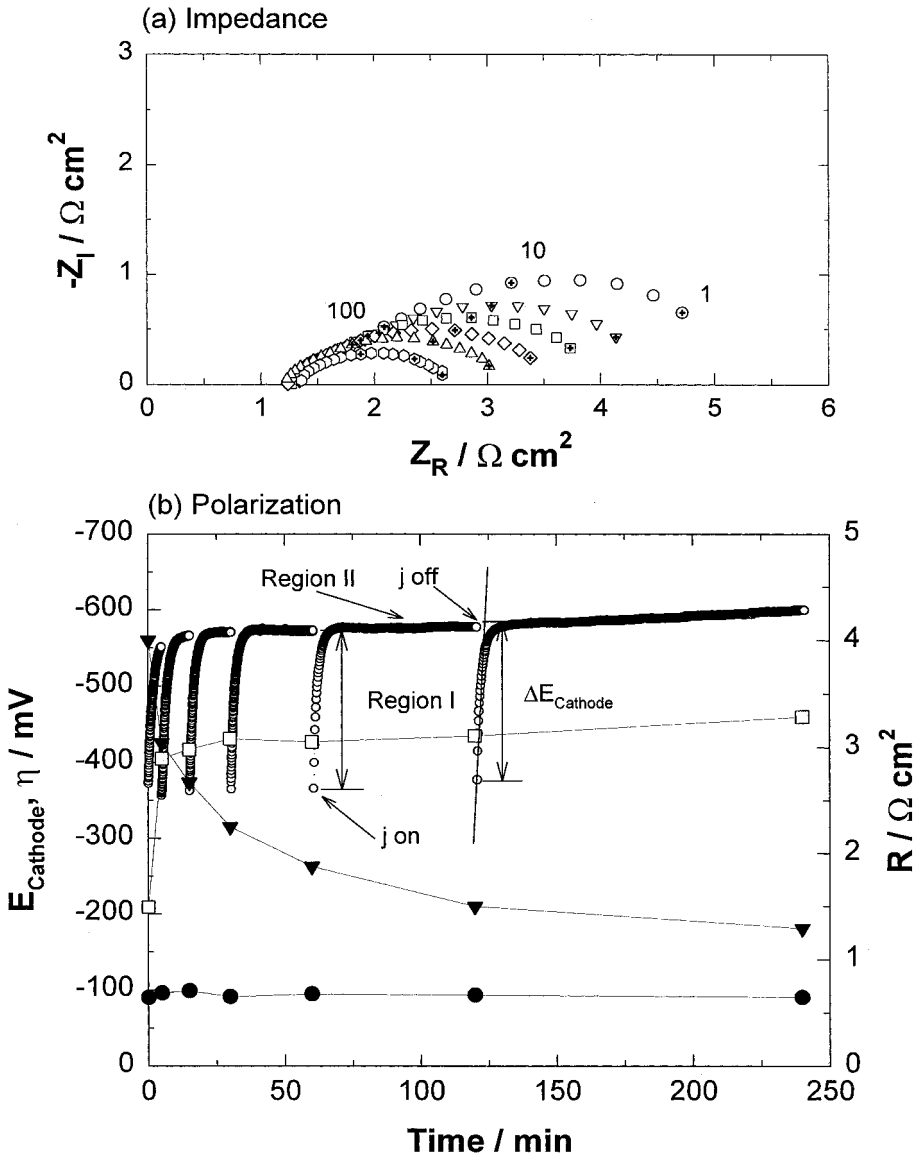

Fig. 4. Initial impedance (a) and polarization (b) curves of a LSM electrode under a cathodic current density of 200 mA cm^{-2} at 900 °C in air in the presence of chromia-forming alloy. Numbers in (a) are frequencies in Hz. Key for (a): (○) 0, (▽) 5, (□) 15, (◇) 30, (△) 60 and (⬭) 240 min. Key for (b): (○) $E_{cathode}$, (□) η, (●) R_Ω and (▼) R_E.

distinct regions I and II. However, the change of $E_{cathode}$ with the current passage is just opposite to that in the absence of chromia-forming alloy. Instead of a rapid decrease, $E_{cathode}$ increased quickly with the current passage in region I, followed by a region II where the increase in $E_{cathode}$ was much slower. Different to that in the absence of chromia-forming alloy, $E_{cathode}$ in region I was almost fully recoverable for the reaction in the presence of chromia-forming alloy. The increase of the initial $E_{cathode}$ with the cathodic polarization current (i.e., $\Delta E_{cathode}$ as shown in the Figure) was 217 ± 9 mV, average of the first five measurements. The instantaneous and fully recoverable behaviour of $E_{cathode}$ with current passage time indicates that the inhibiting effect at the initial stage of polarization is most likely due to the gaseous Cr species rather than the Cr deposit on the TZ3Y electrolyte surface [11]. The change of the $E_{cathode}$ with the current passage time (t) in the presence of chromia-forming alloy is almost the mirror image of that in the absence of the chromia-forming alloy, as shown in Figure 5 of the plots of $E_{cathode}$ against $((t)^{1/2} + t_o)$ where t_o is a constant in order to separate the curves. The very different behaviour of $E_{cathode}$ with the cathodic current passage in the absence and presence of chromia-forming alloy is a clear indication of the significant inhibiting effect of the Cr species on the O_2 reduction at LSM electrodes in the presence of chromia-forming alloy.

Figure 6 is the initial impedance and polarization behaviour of a porous Pt electrode for O_2 reduction under a cathodic current density of 200 mA cm^{-2} at 900 °C in the absence of chromia-forming alloy. The initial R_E was 0.03 Ω cm^2 and η was 8 mV at 200 mA cm^{-2} and 900 °C, indicating high electrochemical activity of Pt for the O_2 reduction reactions. However, $E_{cathode}$ increased steadily with the current

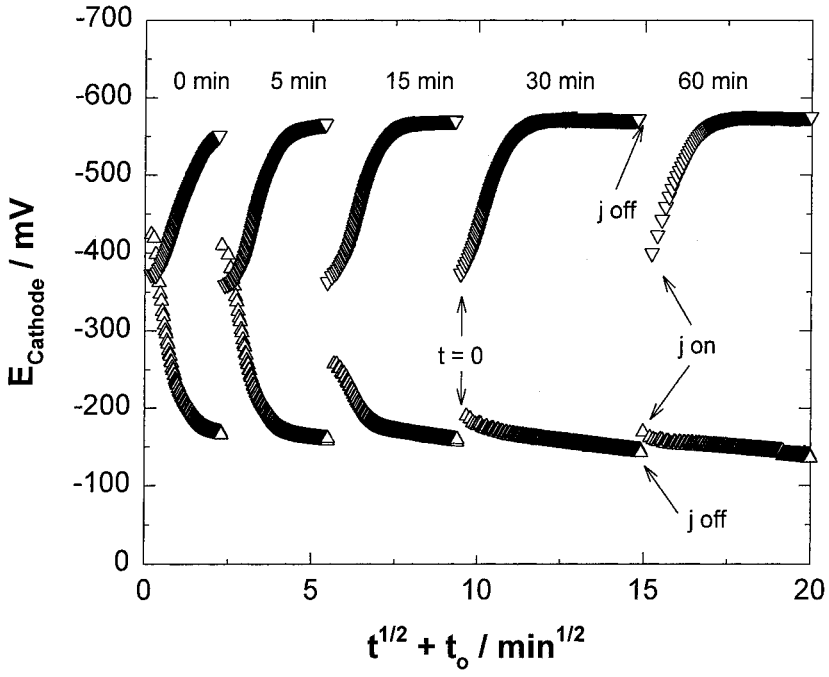

Fig. 5. Plots of $E_{cathode}$ against $((t)^{1/2} + t_o)$ of current passage in the absence ($\triangle$) and presence ($\triangledown$) of chromia-forming alloy, measured at 200 mA cm^{-2} and 900 °C in air. t_o is a constant that separates the plots. The accumulated current passage time before each run is shown in the Figure.

passage time and the increase in $E_{cathode}$ corresponded with the increase in η and R_Ω. The simultaneous increase in η, R_E and R_Ω indicate that the deterioration of the electrochemical activities of the Pt electrode is most likely due to the coarsening of the Pt electrode coating at high temperatures [22]. After the current passage for 60 min, $E_{cathode}$ developed distinct two polarization regions I and II, similar to that observed for the LSM electrodes in the absence of the chromia-forming alloy (Figure 3(b)). Sridhar et al. [23] found that the electrode impedance of Pt was time-dependent and the increase in R_E was attributed to the formation of various oxygen-containing species (OCS) such as Pt–O, which reduces the reaction sites. Thus, the appearance of the potential region I after current passage for 60 min could be related to the formation of various Pt–O species on the Pt electrode surface, and the rapid reduction in $E_{cathode}$ with the cathodic current passage would be an indication of the reduction of Pt–O concentration on the electrode surface [23].

Figure 7 is the initial impedance and polarization curves of a porous Pt electrode for the O_2 reduction at 200 mA cm^{-2} and 900 °C in the presence of chromia-forming alloy. Different from that in the absence of chromia-forming alloy, the distinct two polarization regions I and II occurred instantaneously with the cathodic current passage. η was 213 mV after polarized for 5 min and increased rapidly to 592 mV after polarized for 150 min. However, the magnitude of the initial $E_{cathode}$ increase ($\Delta E_{cathode}$) was rather similar. The average of the first four measurement of $\Delta E_{cathode}$ was 192 ± 13 mV, close to that of the LSM electrode for the O_2 reduction in the presence of chromia-forming alloy. The observation that there was almost no Cr deposition on the surface of Pt electrode and on the surface of the TZ3Y electrolyte indicates that the rapid initial increase in $E_{cathode}$ is most likely due to the inhibiting effect of gaseous Cr species on the O_2 reduction on the Pt electrode. The deterioration of the microstructure of the Pt electrode coating at high temperatures [22] could also contribute to the significant increase of η, similar to that in the absence of chromia-forming alloy.

Figure 8 is the initial impedance and polarization behaviour of a porous LSCF electrode under a cathodic current of 200 mA cm^{-2} at 900 °C in air in the absence of chromia-forming alloy. The impedance spectra measured at open circuit and 900 °C were barely visible, indicating very high electrochemical activity of the LSCF electrode for the O_2 reduction. The high activity was also indicated by the very low η (<10 mV at 200 mA cm^{-2}). In contrast to the LSM and Pt electrodes, there was no appearance or development of the two distinct polarization regions with the current passage for the O_2 reduction on the LSCF electrode. Both impedance and polarization responses were very stable with the current passage time. The very different impedance (R_E) and polarization potential ($E_{cathode}$) behaviour of the LSCF electrode with the cathodic current passage in comparison with that of the LSM and Pt electrodes is most likely related to the high mixed ionic and electronic conductivities of the LSCF-based materials [3] in comparison with the dominant electronic conductivities of LSM and Pt materials [4, 24].

Figure 9 is the initial impedance and polarization behaviour of a porous LSCF electrode for the O_2

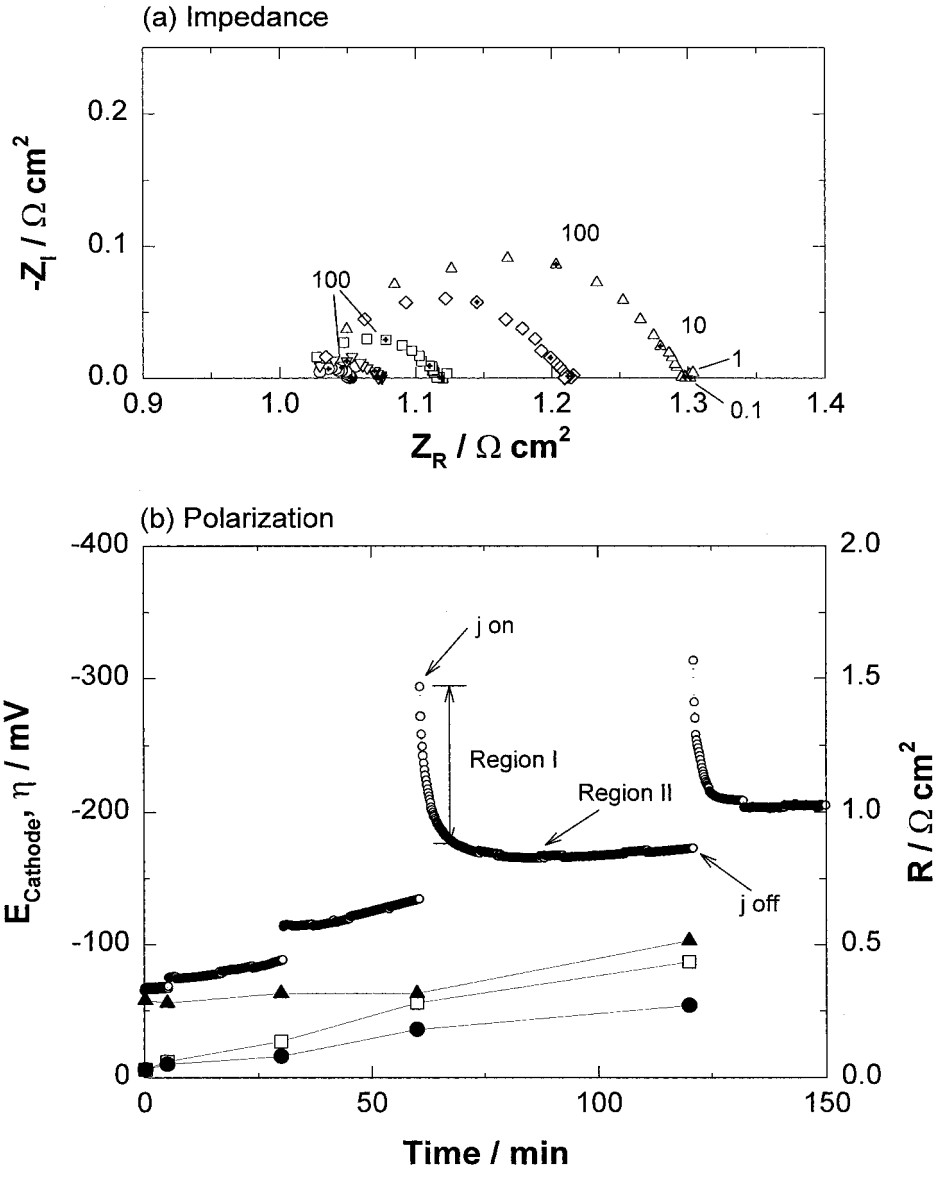

Fig. 6. Initial impedance (a) and polarization (b) curves of a porous Pt electrode under a cathodic current density of 200 mA cm^{-2} at 900 °C in the absence of chromia-forming alloy. Numbers in (a) are frequencies in Hz. Key for (a): (○) 0, (▽) 5, (□) 15, (◇) 60 and (△) 240 min. Key for (b): (○) $E_{cathode}$, (□) η, (●) R_Ω and (▼) R_E.

reduction at 200 mA cm^{-2} and 900 °C in air in the presence of chromia-forming alloy. The impedance arcs were larger than that in the absence of chromia-forming alloy, indicating the increased electrode resistance for the O_2 reduction on the LSCF electrode in the presence of gaseous Cr species. Most interesting, two polarization regions I and II were clearly visible, similar to that observed on the LSM and Pt electrodes in the presence of chromia-forming alloy. However, the magnitude of the initial $E_{cathode}$ increase was much smaller than that on the LSM and Pt electrodes. In average, $\Delta E_{cathode}$ was 13 ± 2 mV, much smaller than 217 ± 9 mV for LSM electrode and 192 ± 13 mV for Pt electrode under identical experimental conditions.

Figure 10 shows the plots of $\Delta E_{cathode}$ against the oxygen diffusion coefficient of the electrodes studied. The average value of $\Delta E_{cathode}$ was measured under current passage of 200 mA cm^{-2} at 900 °C in air in the presence of chromia-forming alloy (for the measurement of $\Delta E_{cathode}$, see Figures 4(b), 7(b) and 9(b)). Oxygen diffusion coefficient values were taken from the literature. For LSCF with composition of $La_{0.5}Sr_{0.5}Co_{0.8}Fe_{0.2}O_3$, oxygen diffusion coefficient is about 5×10^{-7} cm^2 s^{-1} at 900 °C [3]. For LSM materials, the oxygen diffusion coefficient is in the range of 10^{-12} to 10^{-14} cm^2 s^{-1} at 900 °C [3, 4]. Pt is basically impermeable to oxygen ions and its oxygen diffusion coefficient could be as low as 10^{-19} cm^2 s^{-1} at 900 °C if the extrapolation from the high temperature values could be made [24]. $\Delta E_{cathode}$ values for the reaction on LSM and Pt electrodes were close, despite the substantial difference in the microstructure between LSM and Pt electrodes (see Figure 2). As the microstructure difference between LSM and LSCF electrodes would be much smaller than that between LSM and Pt electrodes, the substantial difference in the magnitude of the $\Delta E_{cathode}$

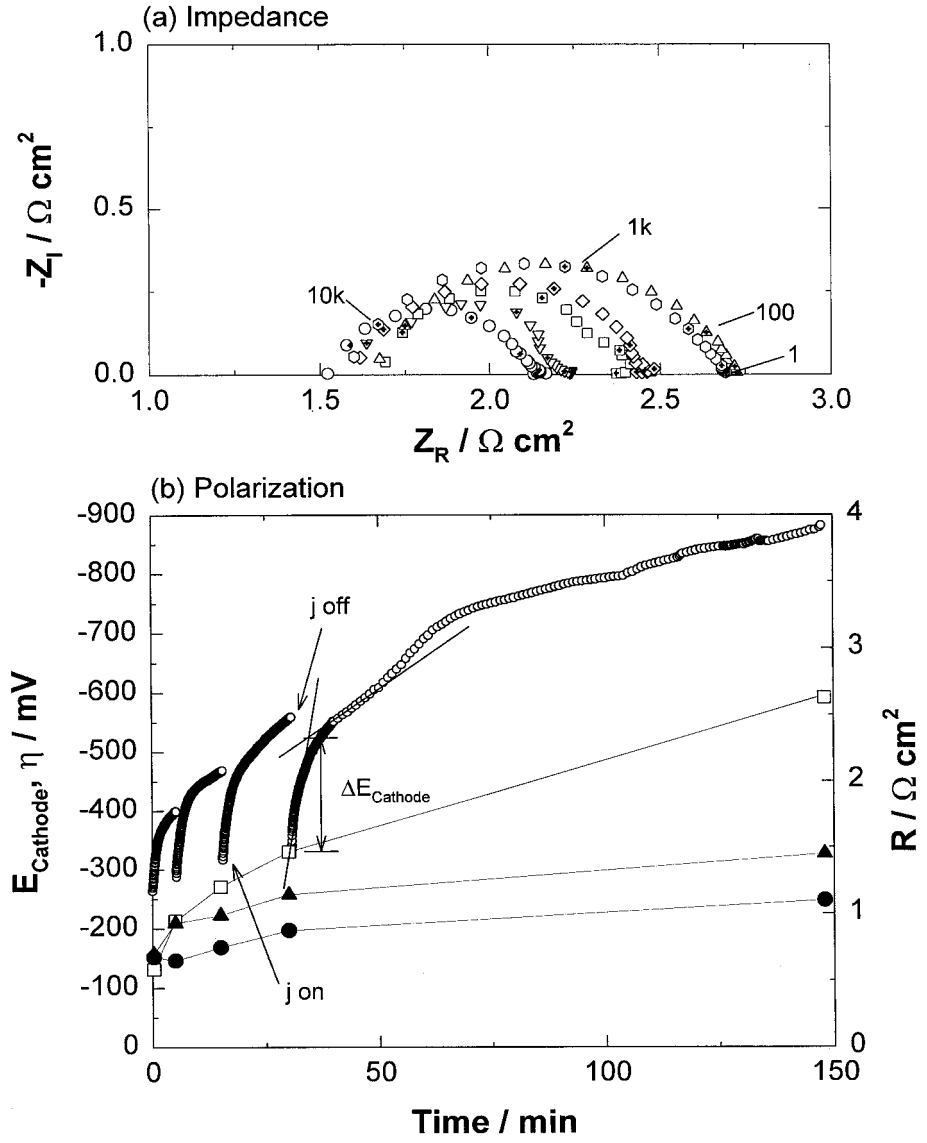

Fig. 7. Initial impedance (a) and polarization (b) curves of a porous Pt electrode under a cathodic current density of 200 mA cm^{-2} at 900 °C in air in presence of chromia-forming alloy. Numbers in (a) are frequencies in Hz. Key for (a): (○) 0, (▽) 5, (□) 15, (◇) 30, (△) 150 and (⬡) 270 min. Key for (b): (○) $E_{cathode}$, (□) η, (●) R_Ω and (▼) R_E.

under identical experimental conditions is an indication of the significant difference in the electrode process for the O_2 reduction on LSCF and LSM electrodes.

3.3. *Effect of gaseous Cr species on surface processes for O_2 reduction*

In principle, all electrode materials can be treated as mixed ionic and electronic conductors (MIECs). The electronic conductivity for LSCF, LSM and Pt electrodes is very high (e.g., > 200 S cm^{-1} at 900 °C) [1]. On the electrode materials studied, LSCF probably has the highest oxygen ion conductivity. Thus, LSCF is a MIEC with significant ionic and electronic conductivities while LSM is a MIEC with dominant electronic conductivity and much smaller ionic conductivity. Similarly, Pt can be treated as a MIEC with almost zero oxygen ion conductivity. Ignoring the details of the elemental steps, O_2 reduction on a porous MIEC electrode can be generally classified into three main pathways [25], as shown in Figure 11. Pathway 1 is the process typically limited by dissociative adsorption and diffusion on the electrode surface (electrode surface process). Pathway 2 is the process limited by the oxygen diffusion through the electrode bulk (electrode bulk process). Pathway 3 is the direct electrochemical reduction of oxygen on the electrolyte surface (electrolyte process) and could occur on the electrolyte surface with some electronic conductivity such as CeO_2-based electrolyte [6]. All three pathways can take place in parallel for the O_2 reduction on a MIEC electrode. Nevertheless, considering that the contribution of the electrolyte process to the overall reaction kinetics would be generally small, the following discussions will be focused on the effect of the gaseous Cr species on the reaction pathways 1 and 2.

Electrode surface process such as surface dissociation and diffusion generally plays an important role for the O_2 reduction on porous LSM electrodes [5, 7, 8]. The

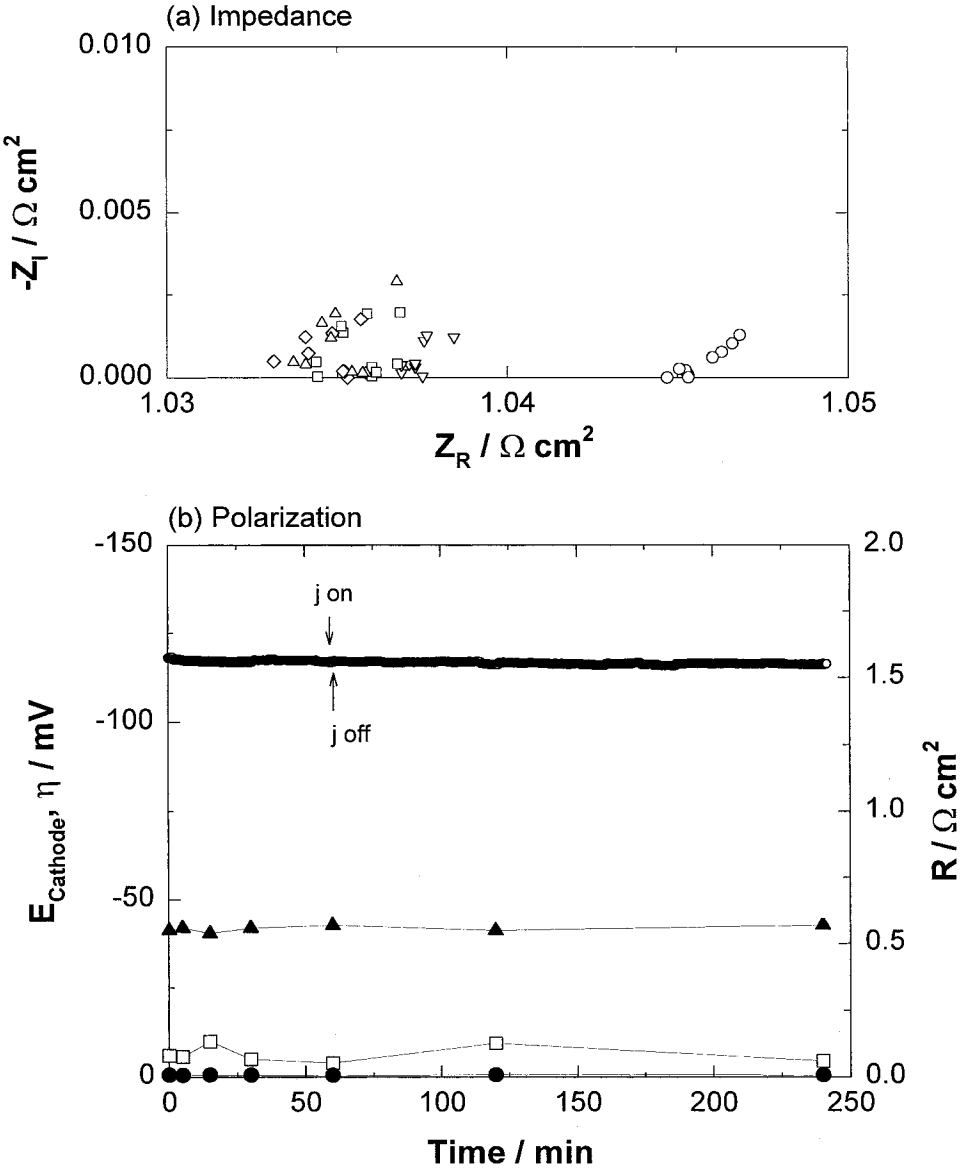

Fig. 8. Initial impedance (a) and polarization (b) curves of a porous LSCF electrode under a cathodic current density of 200 mA cm^{-2} at 900 °C in air in the absence of chromia-forming alloy. Key for (a): (○) 0, (▽) 5, (□) 30, (◇) 120 and (△) 240 min. Key for (b): (○) $E_{cathode}$, (□) η, (●) R_Ω and (▼) R_E.

dominance of the surface process is supported by the significant inhibiting effect of oxygen-containing species (OCS) on the kinetics of the reaction on the LSM electrode. The initial polarization behaviour of LSM electrodes in the absence of chromia-forming alloy shows typical enhancing effect of the cathodic polarization on the electrode process of the O_2 reduction reaction, indicated by the rapid reduction in $E_{cathode}$ with the current passage (Figure 3). The enhancing effect of the cathodic current/polarization is most likely due to the formation of oxygen vacancies on the LSM electrode surface [26]. At early stage of the polarization, the formation of oxygen vacancies could also lead to the decrease and removal of OCS such as SrO and MnO_x originally existed on the electrode surface layer [27]. This is probably indicated by the non-recoverable behaviour of $E_{cathode}$ with the cathodic current passage (Figure 3). The existence of SrO species on the LSM surface is supported by the observation of the surface enrichment of Sr and oxygen contents on the LSM surface [28]. Miura et al. [29] found that removal of SrO segregated to the surface of $La_{0.6}Sr_{0.4}Co_{0.8}Fe_{0.2}O_3$ and $La_{0.6}Sr_{0.4}CoO_3$ membranes by acid etching can improve the oxygen exchange process, resulting in the increase of the oxygen permeation rate through the membrane. Thus the OCS such as SrO originally enriched on the LSM electrode surface could reduce the active sites for the surface dissociative adsorption and diffusion of oxygen, leading to the initially very high R_E and η.

When LSM electrode is in contact with chromia-forming alloy interconnect, gaseous Cr species such as CrO_3 in dry air is produced from the chromium oxide scale formed on the alloy surface [30, 31]. The distribution and concentration of the gaseous CrO_3 species in the electrode system would be primarily affected by the temperature, pressure and the Cr volatility of Cr-containing

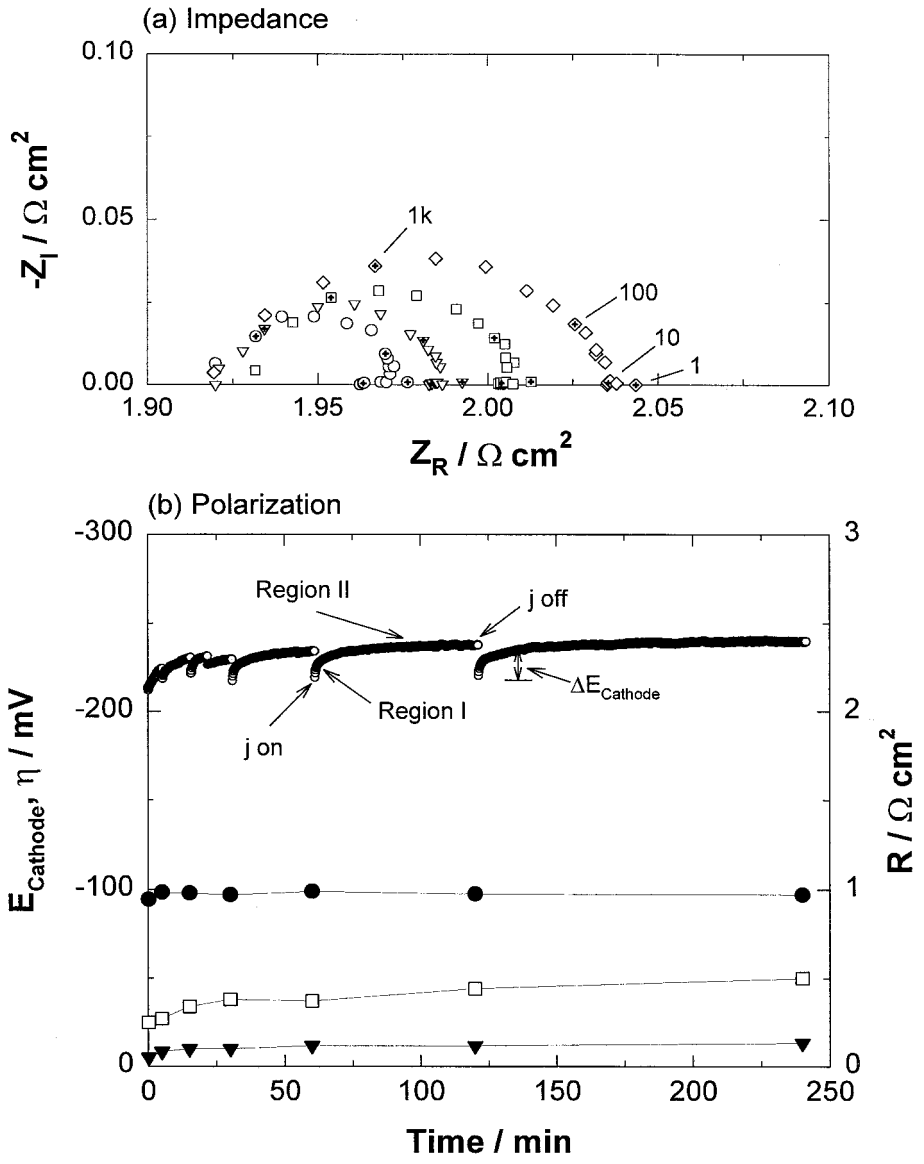

Fig. 9. Initial impedance (a) and polarization (b) curves of a porous LSCF electrode under a cathodic current density of 200 mA cm^{-2} at 900 °C in air in the presence of chromia-forming alloy. Numbers in (a) are frequencies in Hz. Key for (a): (○) 0, (▽) 15, (□) 60 and (◇) 240 min. Key for (b): (○) $E_{cathode}$, (□) η, (●) R_Ω and (▼) R_E.

materials [31]. This means that gaseous Cr species would be a very stable OCS, compared to SrO originally existed on the LSM surface. The inhibiting effect of the gaseous Cr species on the O_2 reduction kinetics is clearly demonstrated by the instantaneous and substantial increase of the polarization potential for the reaction in the presence of chromia-forming alloy, compared to that in the absence of chromia-forming alloy (Figure 5). This indicates that the oxygen vacancies on the LSM electrode surface produced under the cathodic polarization [26] could be quickly occupied by the gaseous Cr species, effectively blocking the diffusion path for the oxygen species on the LSM surface and significantly increasing the resistance for the electrode surface process. The almost fully recoverable $E_{cathode}$ behaviour with current passage time indicates that when current is interrupted the gaseous Cr species could come off the active sites due to the disappearance of the oxygen vacancies, making the active sites available for O_2 diffusion reaction. The above explanation is consistent with the observation that there was no deposition of Cr species on the LSM electrode surface or inside the LSM electrode bulk at the early stage of polarization for the O_2 reduction in the presence of chromia-forming alloy at 900 °C [10].

The effectiveness of the gaseous Cr species in the diagnosing of the surface processes for the O_2 reduction can also be seen on the Pt electrode. Pt is a metallic electrode with very high electronic conductivity and negligible oxygen ion conductivity for the O_2 reduction reactions in SOFC operation conditions. There are convincing evidences that the kinetics of the O_2 reduction on porous Pt electrodes is controlled by the dissociation and/or diffusion of oxygen on the Pt electrode surface even though differences in the elemental steps exist [14–16]. The rapid decrease of $E_{cathode}$ after polarized for 60 min for the O_2 reduction on Pt electrode in the

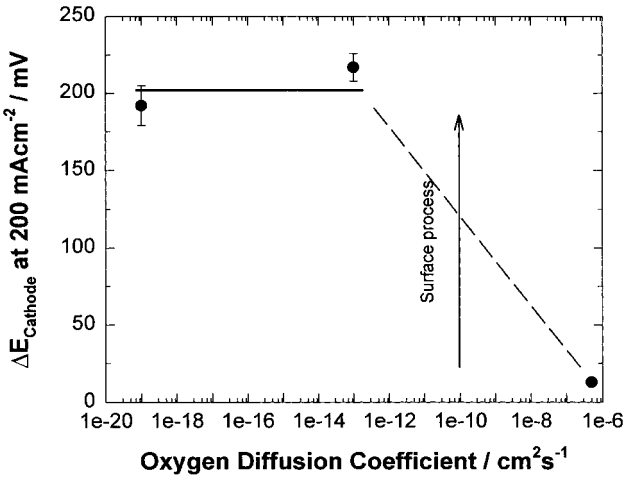

Fig. 10. Plots of $\Delta E_{cathode}$ against oxygen diffusion coefficient of electrode materials for the O_2 reduction in the presence of chromia-forming alloy at 200 mA cm^{-2} and 900 °C. Measurement of $\Delta E_{cathode}$ was given in the text. The lines are intended as guides to the eye.

absence of chromia-forming alloy (Figure 6) can also be attributed to the reduction of the OCS such as Pt–O species existed on the Pt electrode surface [23]. In the presence of chromia-forming alloy, gaseous Cr species could adsorb at the active sites on the Pt electrode surface generated by the reduction of Pt–O species under cathodic polarization potential, effectively blocking active sites for the surface dissociation and diffusion for the reaction on the Pt electrode. The instantaneous and significant increase of $E_{cathode}$ with the current passage time (Figure 7) is a clear evidence of the inhibiting effect of the gaseous Cr species on the surface process. The similar magnitude of the initial increase of $E_{cathode}$ in the presence of gaseous Cr species (see Figure 10) probably provides direct experimental evidence of the dominance of the surface process (pathway 1) on the reaction kinetics for the O_2 reduction on Pt and LSM electrodes. The observation of no deposition of Cr species either on the Pt electrode surface or on the TZ3Y electrolyte

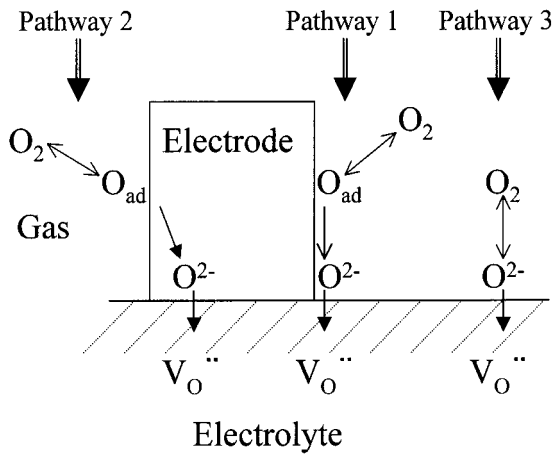

Fig. 11. Scheme of the reaction pathways for O_2 reduction in solid oxide fuel cells.

surface (Figure 2(b)) could also indicate that CrO_3 species may not be electrochemically reduced to Cr_2O_3 during the inhibiting process of the surface process for O_2 reduction on the Pt electrode surface.

LSCF electrode showed much higher electrochemical activity for the O_2 reduction reaction in comparison to LSM and Pt electrodes, indicated by the very low η and $\Delta E_{cathode}$ for the reaction in the presence of chromia-forming alloy interconnect. This is consistent with the observed much higher tolerance of LSCF electrodes towards chromium poisoning than LSM electrodes [32]. Adler et al. [33] analysed the electrode behaviour of LSCF cathodes based on a continuum model and concluded that the O_2 reduction is limited by the surface exchange and bulk diffusion of oxygen (i.e., the electrode bulk process is dominant). Endo et al. [12] studied the electrode performance of dense (~0.8 μm thick) and porous (~50 μm thick) Sr-doped $LaCoO_3$ (LSC) on Sm-doped CeO_2 electrolyte and found that the performance of the porous LSC electrode was significantly higher than the dense LSC electrode. This indicates that the reaction at the gas–electrode–electrolyte three phase boundaries and thus the surface process could also play an important role in the overall reaction kinetics on MIEC electrodes such as LSCF [34]. As shown for the O_2 reduction on the LSM and Pt electrodes, gaseous Cr species significantly inhibit the surface process of the reaction. Also, as indicated previously [10, 11], deposition of Cr species is not dominated by the electrochemical reduction of high valent Cr species in competition with O_2 reduction reactions. Thus, the appearance of the two distinct polarization regions I and II for the reaction on the LSCF electrode in the presence of chromia-forming alloy (Figure 9), similar to that observed on LSM and Pt, confirms that the reaction kinetics are affected by the surface process. The much smaller $\Delta E_{cathode}$ compared to that on the LSM and Pt electrodes measured under 200 mA cm^{-2} at 900 °C (Figure 10) indicates that O_2 reduction on LSCF electrodes is dominated by the electrode bulk process (pathway 2) and to a less extent by the electrode surface process (pathway 1). However, the surface process such as the dissociation adsorption and surface diffusion needs to be taken into account in the consideration of the overall reaction kinetics for the O_2 reduction on a MIEC electrode as indicated by Liu [34].

As discussed above, the kinetics of the surface process (pathway 1) for the O_2 reduction could be quantitatively assessed by the magnitude of the initial $E_{cathode}$ change with the cathodic current passage (i.e., $\Delta E_{cathode}$). For LSM and Pt electrodes, $\Delta E_{cathode}$ was between 192 to 217 mV despite the significant difference in the microstructure between LSM and Pt electrodes. For LSCF electrode, $\Delta E_{cathode}$ was 13 mV, much smaller than that on LSM and Pt electrodes. It appears that the higher the $\Delta E_{cathode}$ value (under certain experimental conditions), the more dominant the surface process in the overall O_2 reduction reactions (as shown by the arrow in Figure 10). Quantitatively, for materials with oxygen

diffusion coefficient less than 10^{-12} cm^2 s^{-1} at 900 °C, the O_2 reduction would be dominated by the surface processes (e.g., the surface diffusion). For materials with oxygen diffusion coefficient of greater than 10^{-7} cm^2 s^{-1} at 900 °C such as LSCF, the electrode process kinetics (e.g., the bulk diffusion) would play more dominant role for the reaction, compared to the surface process. The result has demonstrated the effectiveness and feasibility of the gaseous Cr species in the quantitative determination of the electrode surface and bulk process kinetics for the O_2 reduction under SOFC operation conditions. Nevertheless, it is not clear at this stage whether the gaseous Cr species would be able to differentiate the surface reaction steps such as oxygen adsorption, dissociation and surface diffusion under fuel cell operation conditions.

4. Conclusion

An *in situ* diagnostic method to distinguish the surface and bulk process in the overall reaction kinetics for O_2 reduction reactions in SOFC was presented and the effectiveness of the methods was demonstrated for the reaction on LSM, Pt and LSCF electrodes at 900 °C in air. The diagnostic method is based on the observation that gaseous Cr species (e.g., CrO_3 in dry air) exhibits unique inhibiting properties on the surface process such as the dissociation and surface diffusion for the O_2 reduction on LSM electrodes [11]. Gaseous Cr species was introduced to the system by using chromia-forming alloy. The comparative behaviour of the O_2 reduction on LSM, Pt and LSCF electrodes in the absence and presence of gaseous Cr species clearly demonstrates the strong link between the surface process kinetics and the oxygen diffusion coefficient of the electrode materials. The contribution of the surface process to the overall reaction kinetics could be quantitatively measured by the initial change in $E_{cathode}$ (i.e., $\Delta E_{cathode}$) in the presence of gaseous Cr species. The results show that gaseous Cr species can be used as effective diagnostic tool to distinguish *in situ* the surface and bulk diffusion kinetics for the O_2 reduction reaction under SOFC operation conditions.

Acknowledgement

I would like to thank Sam Hou and Darko Milosevic for the preparation of LSM, LSCF and SDC powders, Jason Baigent for the supply of TZ3Y electrolyte discs and Kylie Chapman for the electrode screen-printing. SEM micrographs of the electrodes were taken by Dr Jin-Ping Zhang. Dr Sudath Amarasinghe kindly reviewed the manuscript. Work was performed during secondment to Ceramic Fuel Cells Ltd.

References

1. N.Q. Minh, *J. Am. Ceram. Soc.* **76** (1993) 563.
2. G. Schiller, R. Henne, M. Lang and S. Schaper, *in* S.C. Singhal and M. Dokiya (Eds), 'SOFC-V', PV99-19 (The Electrochemical Society, Pennington, NJ, 1999), pp. 893–903.
3. S. Carter, A. Selcuk, R.J. Chater, J. Kajda, J.A. Kilner and B.C.H. Steele, *Solid State Ionics* **53–56** (1992) 597.
4. I. Yasuda, K. Ogasawara, M. Hishinuma, T. Kawada and M. Dokiya, *Solid State Ionics* **86–88** (1996) 1197.
5. G.E. Youngblood, A.S. Rupaal, L.R. Pederson and J.L. Bates, *in* S.C. Singhal and H. Iwahara (Eds), 'SOFC-III', PV93-4 (The Electrochemical Society, Pennington, NJ, 1993), pp. 585–597.
6. M. Gödickemeier, K. Sasaki, L.J. Gauckler and I. Riess, *J. Electrochem. Soc.* **144** (1997) 1635.
7. E. Siebert, A. Hammouche and M. Kleitz, *Electrochim. Acta* **40** (1995) 1741.
8. J. Mizusaki, H. Tagawa, K. Tsuneyoshi and A. Sawata, *J. Electrochem. Soc.* **138** (1991) 1867.
9. M. Kuznecov, P. Otschik, K. Eichler and W. Schaffrath, *Ber. Bunsenges. Phys. Chem.* **102** (1998) 1410.
10. S.P. Jiang, J.P. Zhang, L. Apateanu and K. Foger, *J. Electrochem. Soc.*, in press.
11. S.P. Jiang, J.P. Zhang and K. Foger, *J. Electrochem. Soc.*, **147** (2000) 3195.
12. A. Endo, S. Wada, C.-J.Wen, H. Komiyama and K. Yamada, *J. Electrochem. Soc.* **145** (1998) L35.
13. B.C.H. Steele and J-M. Bae, *Solid State Ionics* **106** (1998) 255.
14. J. Mizusaki, K. Amano, S. Yamauchi and K. Fueki, *Solid State Ionics* **22** (1987) 313.
15. J. Mizusaki, K. Amano, S. Yamauchi and K. Fueki, *Solid State Ionics* **22** (1987) 323.
16. C. Schwandt and W. Weppner, *J. Electrochem. Soc.* **144** (1997) 3728.
17. C.C. Chen, M.M. Nasrallah and H.U. Anderson, *in* S.C. Singhal and H. Iwahara (Eds), 'SOFC-III', 'PV 93-4' (The Electrochemical Society, Pennington, NJ, 1993), pp. 252–66.
18. S.P. Jiang and S.P.S. Badwal, *J. Electrochem. Soc.* **144** (1997) 3777.
19. S.P. Jiang, J.P. Zhang and X.G. Zheng, in preparation.
20. W.J. Quadakkers, H. Greiner, M. Hansel, A. Pattanaik, A.S. Khanna and W. Mallener, *Solid State Ionics* **91** (1996) 55.
21. S.P. Jiang, J.G. Love, J.P. Zhang, M. Hoang, Y. Ramprakash, A.E. Hughes and S.P.S. Badwal, *Solid State Ionics* **121** (1999) 1.
22. S.P.S. Badwal and F.C. Ciacchi, *Solid State Ionics* **18–19** (1986) 1054.
23. S. Sridhar, V. Stancovski and U.B. Pal, *Solid State Ionics* **100** (1997) 17.
24. L.R. Velho and R.W. Bartlett, *Met. Trans.* **3** (1972) 65.
25. E. Siebert, *Electrochim. Acta* **39** (1994) 1621.
26. H.Y. Lee, W.S. Cho, S.M. Oh, H.-D. Wiemhöfer and W. Göpel, *J. Electrochem. Soc.* **142** (1995) 2659.
27. S.P. Jiang and J. Love, *Solid State Ionics*, submitted.
28. P. Decorse, G. Caboche and L-C. Dufour, *Solid State Ionics* **117** (1999) 161.
29. N. Miura, Y. Okamoto, J. Tamaki, K. Morinaga and N. Yamazoe, *Solid State Ionics* **79** (1995) 195.
30. D. Caplan and M. Cohen, *J. Electrochem. Soc.* **108** (1961) 438.
31. K. Hilpert, D. Das, M. Miller, D.H. Peck and R. Weiss, *J. Electrochem. Soc.* **143** (1996) 3642.
32. J.G. Love and P.K. Srivastava, 'The Influence of Cathode Performance on the Rate of Chromium Poisoning', Proceedings of the 12th IEA SOFC workshop: 'Materials and Mechanisms', Wadahl, Norway, 10–13 Jan. (1999), pp. 87–90.
33. S.B. Adler, J.A. Lane and B.C.H. Steele, *J. Electrochem. Soc.* **143** (1996) 3554.
34. M. Liu, *J. Electrochem. Soc.* **145** (1998) 142.